Journal of the Mechanics and Physics of Solids 61 (2013) 652–673

Contents lists available at SciVerse ScienceDirect

Journal of the Mechanics and Physics of Solids

journal homepage: www.elsevier.com/locate/jmps

Mechanism of friction in rotating carbon nanotube bearings

Eugene H. Cook [a], Markus J. Buehler [b,*], Zoltan S. Spakovszky [c]

[a] The Charles Stark Draper Laboratory, Inc., Cambridge, MA 02139, USA
[b] Laboratory for Atomistic and Molecular Mechanics (LAMM), Department of Civil and Environmental Engineering, Massachusetts Institute of Technology, Cambridge, MA 02139, USA
[c] Department of Aeronautics and Astronautics, Massachusetts Institute of Technology, Cambridge, MA 02139, USA

ARTICLE INFO

Article history:
Received 1 April 2012
Received in revised form
5 July 2012
Accepted 7 August 2012
Available online 28 August 2012

Keywords:
Carbon nanotubes
Friction
Molecular dynamics
Rotation

ABSTRACT

Simulation of friction in carbon nanotube (CNT) bearing systems has been a popular topic, yet many questions remain open. For example, quantitative estimates of friction reported to date range by as much as eight orders of magnitude, and simulation techniques employ a variety of disparate simulation paradigms and parameters. This paper presents a new suite of consistently implemented but complementary and independent molecular simulations of rotary CNT bearing systems, which span the approaches reported to date, yet agree quantitatively within the error margin, or about one order of magnitude. A comparison between these new results, existing simulation results, and one experimental friction datum is presented. Furthermore, quantitative relationships between friction and the system operating parameters are determined. Friction is found to vary linearly with rotating speed and system temperature, while system length and mean diameter do not have a strong effect. Finally, based on phonon energy spectrum computations, we show that friction is a broadband phenomenon, which does not depend strongly on a specific vibrational mode, but rather appears to occur from the aggregate interactions of many modes at different frequencies. This work reports an in-depth analysis of the mechanics of CNT friction and shows that it can be simulated using complementary approaches, while still obtaining the same result. The analysis reveals the underlying mechanism causing friction and how the governing parameters affect its behavior.

1. Introduction

Friction in carbon nanotubes (CNTs) has been examined using molecular dynamics simulations (Akita and Nakayama, 2003; 2005; Guo and Gao, 2005; Guo et al., 2003; Guo et al., 2005; Liu and Zhang, 2011; Omata et al., 2005; Rivera et al., 2003; Rivera et al., 2005; Servantie and Gaspard, 2006; Zhang et al., 2004; Zhang et al., 2007; Zhu and et al., 2008) and in some experimental studies (Akita and Nakayama, 2003; 2005; Bourlon et al., 2004; Cumings and Zettl, 2000; Fennimore et al., 2003; Kis et al., 2006; Yu et al., 2000; Zettl et al., 2004). However, the values for friction reported in the literature do not agree and show scatter over many orders of magnitude, which makes it difficult to use the data with confidence. Furthermore, the need for a description of the mechanisms causing the friction, as well as knowledge of the dependence of friction on the configuration and operating conditions of an individual CNT-based system (such as a rotating CNT bearing), remains outstanding. The work reported in this paper attempts to address these questions, by performing a broad suite of

* Corresponding author.
E-mail address: mbuehler@mit.edu (M.J. Buehler).

0022-5096/$ - see front matter © 2012 Elsevier Ltd. All rights reserved.
http://dx.doi.org/10.1016/j.jmps.2012.08.004

molecular dynamics simulations of diverse configurations and parameter sets, in a consistent and controlled manner. The goals are to establish the relative importance of and quantitative dependence on the system parameters, to identify the causes of the discrepancies in the literature, and to identify the underlying mechanisms causing the friction from a fundamental perspective. This work presents for the first time a comparison of the existing CNT bearing simulation literature, a consistently implemented array of simulations spanning the parameter space of that literature, and analysis of how the phonons contribute to the interaction of multi-wall CNTs (MWNTs), providing new insight about the mechanisms driving friction. We also report a comparison with the one existing experimental datum on rotating CNT friction (Bourlon et al., 2004).

The unique structure of CNTs has made them interesting as a candidate bearing system, proposed already a short time after their discovery (Charlier and Michenaud, 1993). MWNTs have remarkable strength, owing to the strong covalent bonds joining carbon atoms within each individual tube wall. At the same time, the interactions between adjacent walls are very weak in comparison, due only to van der Waals interactions. Because of this weak interaction, it is universally agreed that CNTs should exhibit "low" resistance to relative motion between these walls; however, quantifying the friction has been difficult. Many research groups have endeavored to determine what the resistance force, or friction, is, and on what parameters it depends. This research also invoked fundamental discussions about the molecular nature of friction and how such atomistic mechanisms relate to the macroscopic concepts known for centuries. Many of these earlier studies have used atomistic simulations to address the problem (Akita and Nakayama, 2003; 2005; Guo and Gao, 2005; Guo et al., 2003; Guo et al., 2005; Omata et al., 2005; Rivera et al., 2003; Rivera et al., 2005; Servantie and Gaspard, 2006; Zhang et al., 2004; Zhang et al., 2007; Zhu and et al., 2008), while a few experimental investigations have also been performed (Akita and Nakayama, 2003; 2005; Bourlon et al., 2004; Cumings and Zettl, 2000; Kis et al., 2006; Yu et al., 2000).

However, the exact magnitude of this friction remains a point of contention. In fact, the values of friction reported in the literature vary by almost eight orders of magnitude, as illustrated in Fig. 1. These data points have been converted from the literature. One issue that arises when trying to compile all the friction data scattered throughout the literature is the use of different units and conventions among the different reports. Conversion of units is typically not a challenge, but in some cases, the units used are not directly compatible, and some ambiguity exists with regard to what exactly is being reported. For example, the friction is commonly quoted in two different ways. Some authors report friction as a shear force, that is, in units of force per area. Other authors report it as a force per atom. In order to convert between the two, it is necessary to know the number of atoms in a unit area, and furthermore whether "per atom" means per atom in a single tube participating in the tube–tube interface, or per the total atoms in the system. The latter has been assumed in converting the data, since it is more consistent with friction being an interfacial property. The number of atoms per area of interface (which should remain within a narrow range independently of tube diameter, even though some variation may occur as bonds stretch and bend) has been taken to be 0.8009 atoms per $Å^2$, based on the geometry simulated here. The other data from the literature used when assembling this comparison (namely sliding speed and temperature) were also inferred or calculated from the papers where not explicitly specified.

Some of the variation in the reported values can be attributed to the different definitions of friction, and to the different approaches used to measure it. In some atomistic simulation studies, molecular statics have been used to study the friction (Akita and Nakayama, 2003; 2005; Guo and Gao, 2005; Guo et al., 2003; Guo et al., 2005; Rivera et al., 2003; Zhang et al., 2004). In these approaches, individual walls of MWNTs are displaced relative to each other either along the tube axis

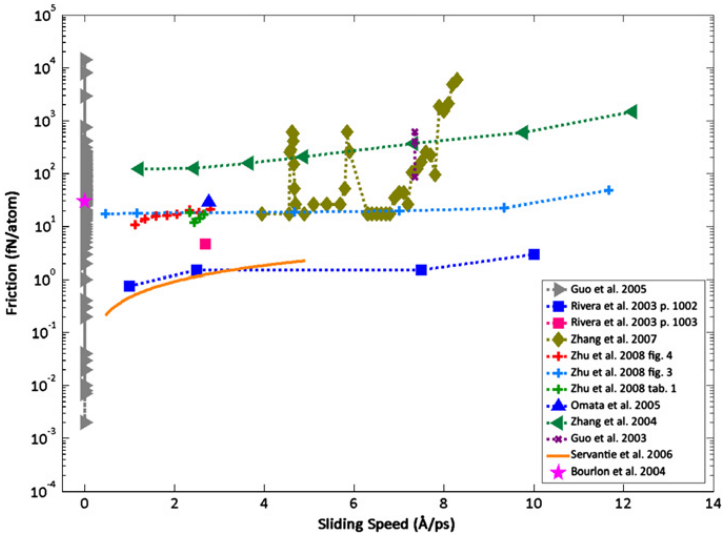

Fig. 1. Friction in the CNT system as reported in the literature, as a function of sliding speed at the interface. The reported results vary by as much as eight orders of magnitude.

(translational motion) or around the tube circumference (rotation). For each displacement step, the energy of the system is measured, in some studies after relaxation of the system. The result of this calculation is a potential energy map, describing the energy as a function of the translational and rotational degrees of freedom (Salehinia and Medyanik, 2011). Then, using this energy versus displacement data, the force or torque is computed as the numerical derivative of the energy with respect to displacement. We have computed these types of potential energy maps, and an example is included in the supplementary material published online with this paper.

There are two limitations with this approach. First, the calculations are time independent, and do not capture any dynamic effects. Since a substantial portion of the interaction between walls of a MWNT may be due to phonons in one tube exciting phonons in the other, the treatment of this interaction as a static phenomenon may not be warranted. Second, because the energy in the system is computed based on a potential, and the force is the derivative of this potential, the force must be conservative, by construction. For example, integrating this torque about a complete revolution in a rotating system yields identically zero:

$$\int_{\theta_0}^{\theta_0+2\pi} \frac{dE}{d\theta} \equiv 0. \tag{1}$$

This tautology indicates that there can be no energy dissipation when considering only these potential resistance forces in a static manner. Friction is not conservative, but rather dissipative. Thus, this resistance force cannot be equated to the friction. The distinction between these gradient-based forces, which are also sometimes called corrugations, and friction in a system experiencing fully dynamic motion, immediately explains some of the discrepancies among the reported literature. These two types of forces are different quantities, and should not be expected to correlate directly.

Recognizing the limitations of the static analyses, some of the aforementioned studies (Guo et al., 2003; Rivera et al., 2003; Zhang et al., 2004), as well as others (Guo and Gao, 2005; Guo et al., 2005; Omata et al., 2005; Rivera et al., 2005; Servantie and Gaspard, 2006; Zhang et al., 2007; Zhu and et al., 2008), have used molecular dynamics to simulate such systems. In these simulations, the equations of motion based on the empirical potential are integrated in time, resulting in a trajectory for each atom. For some works (Zhang et al., 2004; Zhang et al., 2007; Zhu and et al., 2008), a steady-state approach has been used, wherein a constant relative velocity (Zhang et al., 2004; Zhu and et al., 2008) or force (Zhang et al., 2007) is applied to the tube walls. Other works (Guo and Gao, 2005; Guo et al., 2003; Guo et al., 2005; Omata et al., 2005; Rivera et al., 2003; Rivera et al., 2005; Servantie and Gaspard, 2006) have elected to study unsteady situations, with no constraints on the relative motion of the tube. In these cases, the speed or amplitude of the motion decays with time as friction transfers energy from the orderly overall motion into random thermal motions.

While both translational and rotational motions have been addressed in the existing literature, for this work it was decided to concentrate on rotational motion in carbon nanotubes. Translational motions must contend with a restoring force due to van der Waals interactions: the van der Waals energy in the system decreases as the contact area between adjacent walls of the MWNT increases. Thus, when walls are displaced axially, there is a force that tends to increase the contact area by aligning the walls in the axial direction. Rotational motions do not exhibit this force, because the contact area does not change as one tube rotates within another. Rotational motion was therefore selected in order to eliminate this force, which could be difficult to distinguish from a true friction force. Furthermore, rotational motions do not experience strong effects due to edge–edge interactions, as translating systems can (Guo et al., 2011). Additionally, by constraining the motion of the tube to rotation only, the complicating effects of any coupling between rotation and translation can be eliminated. Considering only the literature which addresses rotation in a dynamic way (Omata et al., 2005; Servantie and Gaspard, 2006; Zhang et al., 2004; Zhu and et al., 2008), the range of predicted friction forces is dramatically decreased, from eight orders to only three (as can be seen in Fig. 7, compared with the results of this study); however, the reason for the remaining discrepancy has not yet been explained. It is the goal of the present work to illustrate that this discrepancy can be avoided, even when comparing results from different and independent simulation techniques. It will be shown that by emphasizing consistency of implementation across the different simulation types, the agreement can be better than one order of magnitude.

1.1. Outline

Having introduced the problem and discussed the related literature, we will first lay out the methods used to perform the new simulations for this work. The tool implementation and common simulation parameters (such as geometry and time step) are described first, followed by a description of the specific boundary and initial conditions that define the four complementary simulation types used (quasi-steady adiabatic, steady isothermal, spin-up, and coast-down). Then we will describe the tools used to extract and process the phonon spectra. The Results and Discussion section will present the findings of the simulations. First, the new results will be compared with the existing literature, to establish the level of agreement between the different simulations done here and previously. Next, we will describe a series of parametric studies, in which the simulation parameters are swept through a range, to determine the relationship between each parameter and the friction in the system. Finally, the results of the phonon spectra calculations will be presented, and the implications for the mechanism causing friction will be discussed.

2. Materials and methods

2.1. Simulation tools

For the present work, simulations were carried out using the Large-scale Atomic/Molecular Massively Parallel Simulator (LAMMPS) code (2010; Plimpton, 1995). For a force field, the Adaptive Intermolecular Reactive Empirical Bond Order (AIREBO) potential (Stuart et al., 2000) was used. This potential, which was designed for molecules comprised of carbon and hydrogen, is based on an earlier empirical potential by Brenner (1990), which describes the interactions between covalently bonded carbon and hydrogen atoms. It also includes four-body terms, which account for energy changes due to torsion of the bonds between atoms, about their equilibrium positions. In addition, the LAMMPS implementation of this potential includes a Lennard-Jones (1931) style potential term, used to model the long range van der Waals type interactions between atoms not within the same molecule.

Except where otherwise noted, an integration time step of 1 fs has been used; this time step is about one order of magnitude smaller than the timescale of the fastest phonons (Tersoff, 1988), and so should adequately capture all the relevant dynamics. The baseline starting point geometry (about which other variations in geometry were later explored) is shown in Fig. 2 and consisted of a (9,9) CNT inside a (14,14) CNT, with lengths of 60 nm and 50 nm and radii of 0.619 nm and 0.963 nm, respectively; these comprise 886 and 1120 atoms, respectively. The spacing between walls is 0.3438 nm, which agrees well with the known equilibrium distance between CNT walls, an important consideration to ensure that the simulation accurately approximates nature. This geometry was selected because it is representative of the geometries used in the literature.

At the beginning of each simulation, following an energy minimization, the tubes were allowed to equilibrate under a Langevin-style thermostat to 300 K before any rotation was introduced. Rotation was simulated at rates between 25 and 250 GHz. On the low speed end, the limitations are computational cost (the length of real time required to run the simulation is proportional to the simulated time), as well as noise; at low speeds, the energy in thermal motion is of the same order as for the faster speeds, but the energy in rotation and the energy transfer rate due to friction are lower, and it is thus more difficult to distinguish the friction signal from the noise. The problem can be addressed by increasing the simulation length (to increase the total friction work done) or simulating multiple systems and averaging to reduce noise, both of which also compound the computational cost. On the fast end, the limitation is the structural integrity of the tube; as the rotation becomes faster, centrifugal forces as well as torque applied by the boundary conditions to enforce rotation become strong enough to break bonds within the tube. The threshold for this type of failure has been reported to be around 500–750 GHz (Zhang et al., 2004).

2.2. Simulation types

One main goal of the simulations is to demonstrate that friction estimates that agree quantitatively can be obtained even from different simulation techniques. Four different techniques have been employed here, which span the possible techniques reported in the selected literature (Omata et al., 2005; Servantie and Gaspard, 2006; Zhang et al., 2004; Zhu and et al., 2008) as well as one new technique (spin-up). Table 1 summarizes the key differences between these simulation types, including the boundary and initial conditions (shown geometrically in Fig. 2) and the parameters and equations used to compute the friction.

2.3. Steady isothermal

One method of determining the friction in a CNT system is to set it rotating into steady rotation, and to extract the friction at this steady state condition. For this method, the inner tube rotated at a constant angular velocity, while the

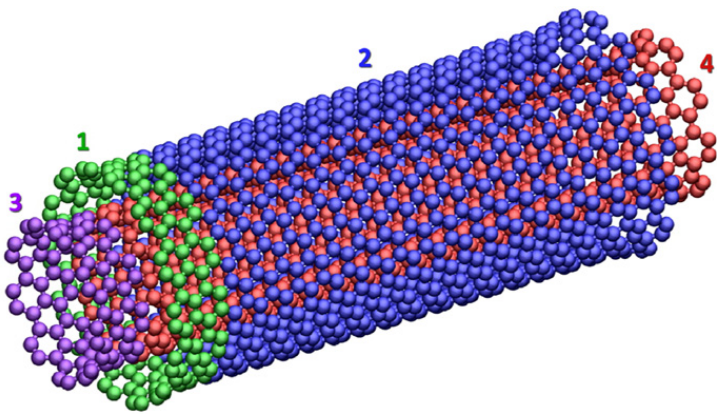

Fig. 2. Boundary condition regions in the baseline geometry (a 60 nm (9,9) CNT centered in a 50 nm (14,14) CNT).

Table 1
Comparison of simulation types[a].

Simulation type		Steady isothermal Steady state	Quasi-steady adiabatic Steady state	Coast-down Transient	Spin-up Transient
Boundary conditions	**1**	Fixed	Fixed	Free	Free
	2	Thermostated	Free	Free	Free
	3	Spinning	Spinning	Free	Spinning
	4	Free	Free	Free	free
Initial conditions	**1**	Motionless	Motionless	Temperature	Temperature
	2	Temperature	Temperature	Temperature	Temperature
	3	Spinning	Spinning	Spinning	Spinning
	4	Temperature	Temperature	Spinning	Spinning
Friction extracted from		Energy exchange at thermostat	Energy accumulation	Angular momentum change	Angular momentum change OR Energy accumulation
Friction measurement equation		$\dot{E} = F_f r_I \Omega$		$\frac{dL}{dt} = \pm F_f r_I$	

"Temperature" initial condition indicates that the atoms have random thermal motion, but no orderly bulk motion (*i.e.* rotation).
[a] Numbers listed next to boundary and initial conditions correspond to regions of the CNT identified in Fig. 2.

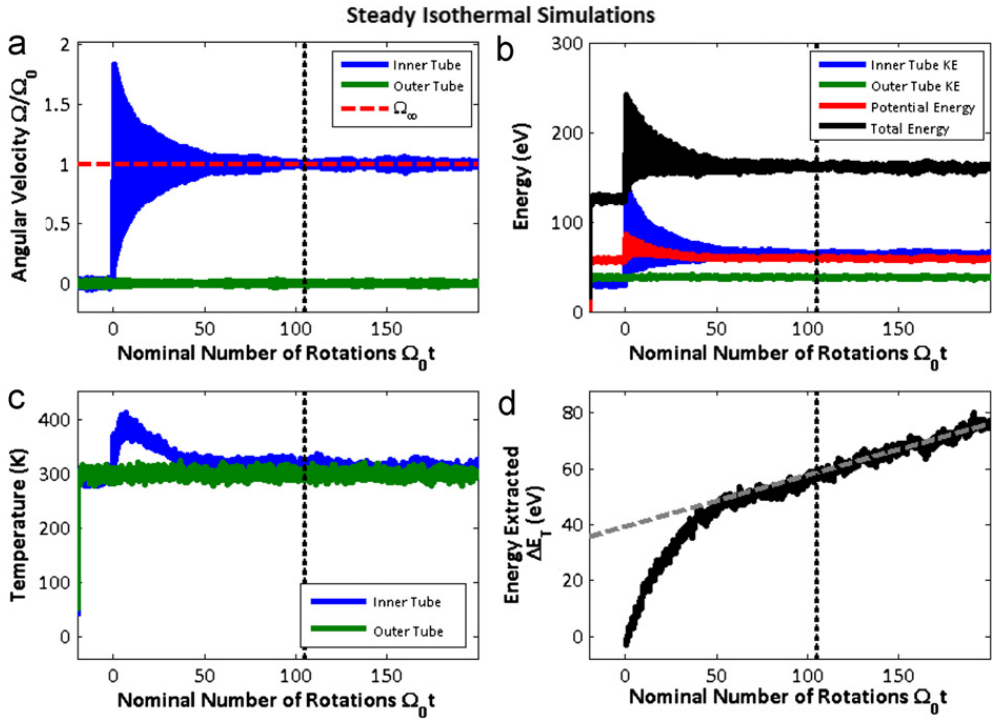

Fig. 3. Example data collected from an isothermal constant velocity simulation at 200 GHz, showing angular velocity (a), temperature (c), and kinetic energy (b) of each tube, along with other energies (b) and the running total of energy extracted via the thermostat (d). The dashed vertical lines represent the end of the startup transient and the beginning of the region used for fitting.

outer tube was held fixed. These constraints were accomplished by enforcing zero velocity or the prescribed angular velocity on a few rings of atoms at one end of each tube. A Nosé–Hoover-style thermostat (Hoover, 1985; Nosé, 1984), was applied to the outer tube, to simulate contact with a large heat reservoir, also at 300 K. The simulation can therefore be referred to as isothermal. After an initial transient, during which the stationary atoms in the center tube accelerate to catch up with the constrained atoms at the tube end, the system reaches steady state. The atoms in the inner tube rotate with approximately uniform speed. Fig. 3(a) clearly shows the transient in the angular velocity, and the eventual steady rotation which results, for an example simulation at 200 GHz. This transient consists mostly of the torsional mode in the rotating CNT, excited by suddenly applying a torque to the end atoms to enforce the rotation rate.

The friction forces tend to slow down the rotating tube by transferring that orderly kinetic energy into random thermal motion. However, the enforced velocity constraint causes the kinetic energy of the inner tube to be maintained, resulting in an accumulation of thermal energy. The thermostat on the outer tube continually extracts heat to maintain the

temperature (Fig. 3(c)). Temperature is computed during the simulation using kinetic theory:

$$T = \frac{m\overline{v}_{\mathrm{T}}^2}{3k_B} \tag{2}$$

where $\overline{v}_T$ is the average thermal velocity of each atom, and m is the atom's mass. The term "thermal velocity" is used to indicate that these velocities are corrected for the bulk motion of the tube, that is, the angular velocity $\vec{\Omega} \times \vec{r}$ is subtracted from each atom's velocity before calculating the average. Atoms that are constrained by boundary conditions are also neglected in the temperature calculation.

At steady state, the total energy is not changing with time (see Fig. 3(b)), so the rate of kinetic energy addition equals the rate of heat extraction, which is also equal to the rate at which the frictional work converts the kinetic energy into thermal energy. Thus, by measuring the rate of heat extraction at the thermostat (example shown in Fig. 3(d)), the friction power and hence the friction is known. This is the same approach used by Zhang et al. (2004).

To compute the friction from the thermostat heat extraction data, it is necessary to compute the rate $\dot{Q}$ at which heat is extracted via the thermostat. For the steady state simulation, this rate is constant, so the total energy extracted,

$$\Delta E_{thermostat} = \int_0^t \dot{Q}\,dt \tag{3}$$

is a linear function of the simulation time. The rate was taken to be the slope of a least squares fit to the portion of the energy extracted data after the transient has damped out. The vertical dotted lines in Fig. 3 mark the time at which the transient was deemed extinguished, and the dashed, sloped line in Fig. 3(d) is the linear fit. The friction power is then equated to the heat extraction rate

$$\dot{Q} = \tau_f \Omega = F_f r_I \Omega \tag{4}$$

allowing the friction toque τ_f and the friction force F_f to be extracted (r_I is the interface radius, or average of the two tube radii, and was measured during each simulation).

2.4. Quasi-steady adiabatic

A variant of the constant velocity method is to eliminate the thermostat on the outer tube, resulting in an adiabatic simulation. The result is that as kinetic energy is continually added, and converted into thermal energy by the friction, the total energy of the system builds up over time (shown in an example simulation in Fig. 4d). The friction power is then equal to the energy accumulation rate. Because energy is accumulating, the system is not strictly in a steady state, as the temperature is increasing with time (Fig. 4c). However, if the change in temperature is small compared to the absolute temperature, and this effect is neglected, the resulting friction is close to the isothermal result. This is the approach used by Zhu and et al. (2008).

Like the isothermal case, the rate of energy change $\dot{E}$ (here built up in the system instead of extracted via thermostat) is constant in the steady state, leading to a linear evolution of the system total energy E, and again the friction is found from

$$\dot{E} = \tau_f \Omega = F_f r_I \Omega \tag{5}$$

Neglecting the temperature change, allowing the simulation to be treated as quasi-steady, is reasonable for low speeds. For example, the 100 GHz case, shown in Fig. 4, experiences a temperature rise of 55 K, or 18% of the original temperature over the course of the simulation. For higher speeds, with higher energy conversion rates, the change is much more. For example, at 250 GHz, the temperature rise is 280 K; the temperature nearly doubles. Therefore, the adiabatic simulation does not effectively isolate the effect of temperature on the friction, particularly at high speeds.

2.5. Coast-down

An alternative method to determine the friction is to allow a rotating CNT to move freely, and observing how the friction affects the evolution of this motion. This method has the advantage that motion need not be imposed on any atoms in the simulation in order to maintain a consistent speed in the presence of friction. Therefore, all the atoms in the simulation are free, and thus experience the proper physics (and not an artificial boundary condition.) However, the drawback is that as a result of the frictional torque, the CNT accelerates or decelerates, and the conditions under which friction is being measured change throughout the simulation. These unsteady simulations have been used as a complement to the steady simulations, with the goal of demonstrating that the same friction value can be computed independent of simulation method.

For the unsteady coast-down simulations, there are no constraints on the walls of the MWNT. Instead, the inner tube is given an initial angular velocity, and the two tubes are allowed to move freely. The friction causes the rotating tube to transfer its angular momentum to the stationary tube, so that the rotating tube slows down and the stationary tube gradually accelerates. The friction is the only torque on either tube, so the friction torque can be found directly as the time

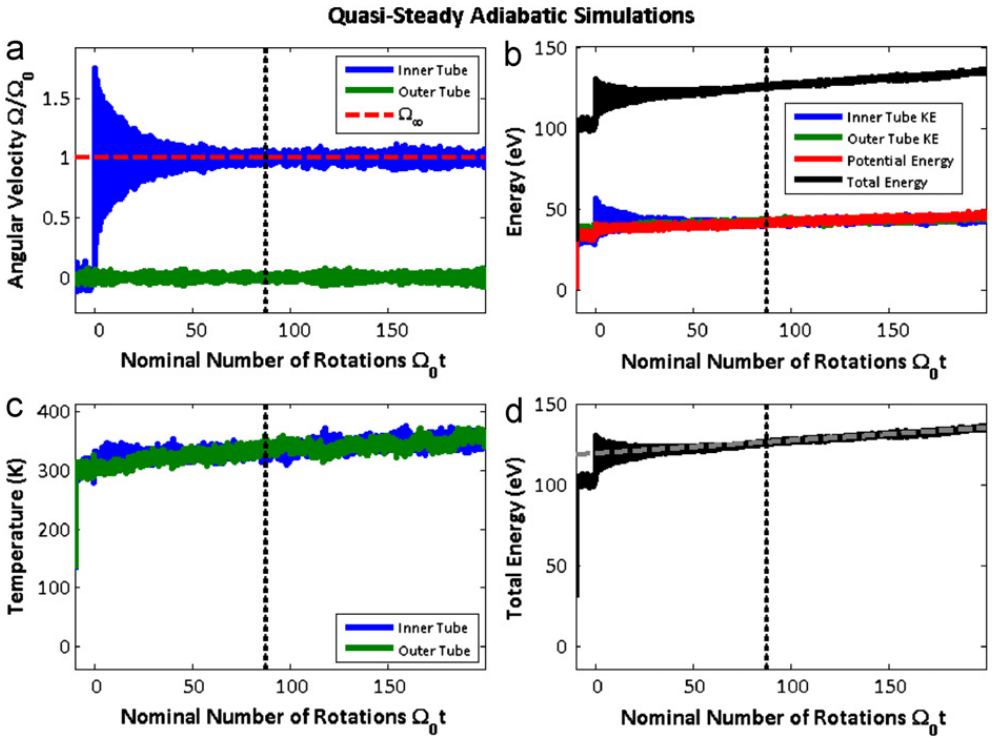

Fig. 4. Example data collected from an adiabatic constant velocity simulation at 100 GHz, showing angular velocity (a), temperature (c), and kinetic energy (b) of each tube, along with other energies (b) and the total energy in the system (d). The dashed vertical lines represent the end of the startup transient and the beginning of the region used for fitting.

rate of change of the angular momentum of either tube:

$$\tau_f = \pm \frac{dL}{dt} \tag{6}$$

where the friction torque τ_f is taken to be positive, and the sign in the equation is therefore positive for the outer tube (initially at rest) and negative for the inner tube (initially rotating). An example angular momentum trace is shown in Fig. 4(d). This is the approach used by Omata et al. (2005) and Servantie and Gaspard (2006).

Because the tubes are accelerating, the angular velocity is not constant in time. There are two possible ways to deal with this issue. If the total change in velocity over the course of the simulation is small with respect to the absolute velocity at the beginning of the simulation, it can be assumed that the friction does not change as a result of velocity changes. Therefore, the friction is constant over the simulation, and the angular momenta of the tubes should vary linearly, with slope equal to that friction:

$$L_1 = L_0 - \tau_f t \tag{7a}$$

$$L_2 = \tau_f t \tag{7b}$$

where L_1 and L_2 are the angular momenta of the inner and outer tubes, respectively; $L_0 = \Omega_0 I_1$ is the initial angular momentum of the inner tube (the outer tube starts at rest and does not contribute to the initial angular momentum). This linear relationship between angular momentum and time (or angular velocity and time, since $\Omega = L/I$) is indeed approximately true for short simulation periods and low friction used. (Equivalently, the approximation is good for small values of the non-dimensional parameter $\tau_f T/I\Omega$, which ranged from 0.5 to 10 for these simulations; values of 1 or less worked the best.) The torque is extracted by fitting a least-squares line to the angular momentum data for each tube, starting just after the rotation; these fits are the dashed lines in Fig. 5(b&d). Throughout the text, we will refer to this as a "linear unsteady fit." The sign of the error introduced by the constant friction assumption is known: this method will under-predict the friction, because the average speed during the simulation is in fact lower than the nominal speed, and hence the friction reported actually corresponds to a slightly lower speed.

However, the assumption breaks down for longer simulations or for lower relative speeds between the tubes. To treat the situation more accurately, we can assume that the friction varies proportionally with the relative angular velocity between the two tubes (as is done by Servantie and Gaspard (2006)), *i.e.*

$$\pm \frac{dL}{dt} = \tau_f = \frac{I_1 I_2}{I_1 + I_2} \lambda (\Omega_1 - \Omega_2) \tag{8}$$

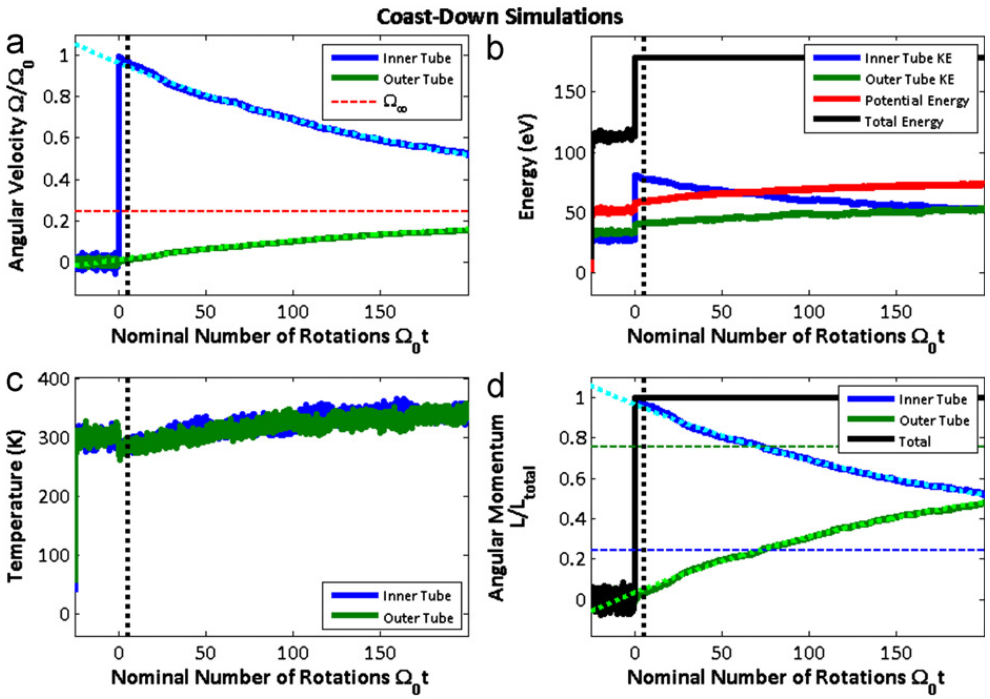

Fig. 5. Angular velocity evolution (a) during an example coast down simulation at 250 GHz. The small initial transient motion is due to the release of the constraints on the end atoms used during thermal equilibration. The rate of change of the angular momentum (d) can be approximated as linear for this short time simulation, or it can be fit with an exponential for longer times; these are shown as dashed and dotted lines, respectively. Temperature (c) and energy (b) are also recorded during the simulation.

where λ is the proportionality constant (which will turn out to be the exponential decay rate of the rotation), and the moments of inertia I_1 and I_2 have been introduced to simplify the algebra later on. We can then use the knowledge that there are no external torques, so angular momentum is conserved in the simulation, or the total angular momentum is always equal to the initial angular momentum:

$$I_1\Omega_1+I_2\Omega_2=L_0 \tag{9}$$

to eliminate one of the angular velocities from the differential equation:

$$\Omega_2=\frac{L_0-I_1\Omega_1}{I_2} \tag{10}$$

$$\begin{aligned}-\frac{dL_1}{dt}=\tau_f&=\frac{I_1I_2}{I_1+I_2}\lambda\,(\Omega_1-\Omega_2)\\&=\frac{B}{I_1+I_2}\left[I_1I_2\Omega_1+I_1^2\Omega_1-I_1L_0\right]\\&=B\left[I_1\Omega_1-\frac{I_1L_0}{(I_1+I_2)}\right]\\&=B\left[L_1-\frac{I_1L_0}{(I_1+I_2)}\right]\end{aligned} \tag{11}$$

The solution is an exponential:

$$L_1=A_1\exp(-\lambda t)+\frac{L_0I_1}{I_1+I_2} \tag{12}$$

We note that at the end of the rotation, friction will have eliminated the relative angular velocity, and both tubes will have the same velocity Ω_f (marked with a red dashed line in Fig. 5(a)), which can again be found by conservation of angular momentum:

$$(I_1+I_2)\Omega_f=L_0=I_1\Omega_0 \tag{13}$$

$$\frac{L_0}{I_1+I_2}=\Omega_f \tag{14}$$

Substituting this into the equation gives

$$L_1=A_1\exp(-\lambda t)+I_1\Omega_f \tag{15}$$

and it can be similarly shown that

$$L_2 = I_2\Omega_f - A_2\exp(-\lambda t) \tag{16}$$

these exponential functions can also be fit to the experimental data, allowing the extraction of the parameter λ, which will always be positive. The exponential fits for angular momentum and angular velocity are the dotted lines in Fig. 5(a&d). Once λ has been determined, the friction at a given rotation rate is computed from

$$\tau_f = \lambda\left[L_1 - \frac{I_1 L_0}{(I_1+I_2)}\right] = \lambda I_1(\Omega_1 - \Omega_f) = \lambda I_2(\Omega_f - \Omega_2) \tag{17}$$

this method will be referred to as an "exponential unsteady fit." Note that the exponential unsteady fitting technique can provide estimates for the friction at any speed from a single run; in later graphs, the speed chosen to demonstrate the results will be the initial speed Ω_0 of each simulation.

Another important note is that because the velocity constraint is released at the beginning of the simulation, and there is no thermostat, the energy in the system is necessarily conserved during these simulations. This is illustrated in Fig. 5 . An important consequence of this is that unlike the quasi-steady adiabatic simulations, where the temperature increases dramatically during the simulation due to the kinetic energy added by the velocity constraint, for the coast down simulation the temperature rise is much more modest. Even for the highest speed (250 GHz,) the temperature increases by only about 43 K, or 14% of the initial temperature.

2.6. Spin-up

An additional type of unsteady simulation was performed wherein the inner, rotating tube is constrained to keep rotating using the same enforced velocity at the tube end as in the constant velocity case. Fig. 6 shows the angular velocity evolution for this case. The outer tube, however, remains free, and gradually accelerates due to the friction torque. The final, asymptotic angular velocity Ω_f is thus equal to the initial angular velocity Ω_0. The friction torque can be measured in the same manner as for the coast-down simulations, that is, by fitting either a linear function

$$L_2 = \tau_f t \tag{18}$$

or exponential function

$$L_2 = I_2[\Omega_0 - A_2\exp(-\lambda t)] \tag{19a}$$

$$\tau_f = \lambda I_2(\Omega_f - \Omega_2) \tag{19b}$$

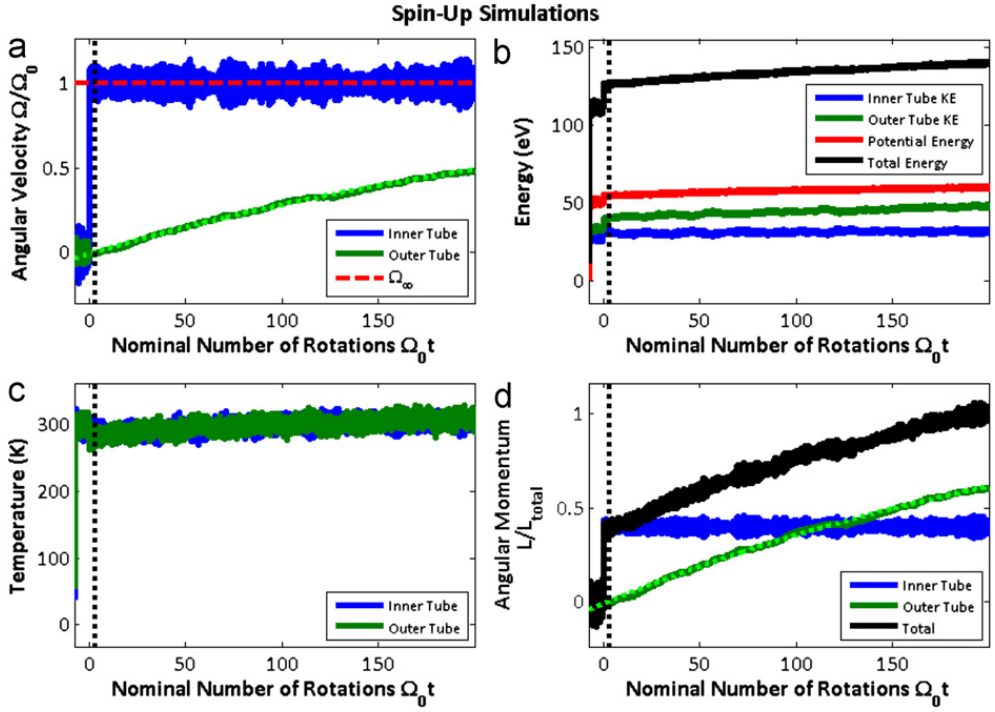

Fig. 6. Angular velocity (a), energy (b), temperature (c), and angular momentum (d) evolution during a spin-up simulation at 75 GHz. The inner tube's angular velocity and angular momentum are held constant, while the outer tube gradually catches up.

to the angular momentum of the accelerating tube, and extracting the constant or velocity-proportional friction value from the fit coefficients. Note that the spin-up simulations suffer from the same temperature increase as the quasi-steady adiabatic simulations, since energy is constantly being added by the enforced velocity boundary condition.

3. Results and discussion

3.1. Comparison with existing literature

The first results of the four simulations types described here, along with the literature selected as most relevant and one experimental datum (Bourlon et al., 2004), are shown in Fig. 7 (and a magnified version in Fig. 8). Error bars, representing the minimum and maximum result over an ensemble of 5 runs with different thermal velocity random seeds, are included. All four strategies agree with each other within less than an order of magnitude, and for most of the range even within the ensemble error bars. This is much better than the three-order variation in the literature. This is an important result, because it illustrates that the variations amongst the literature results are not due to inherent differences in the physics of

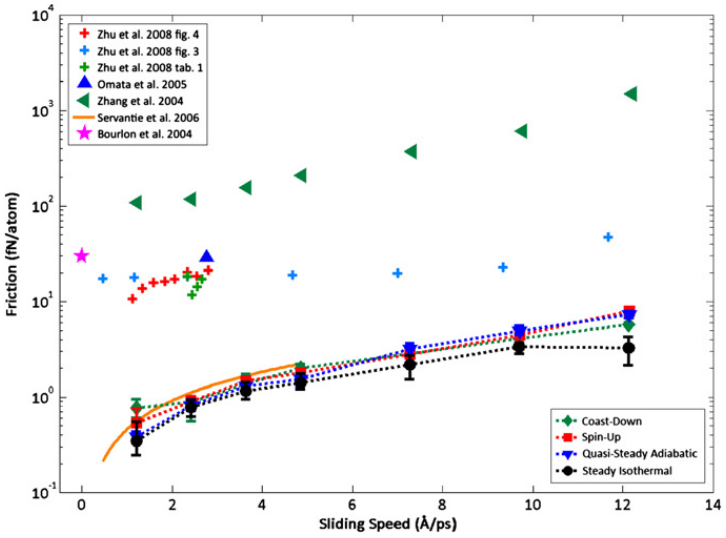

Fig. 7. Results from all the independent simulation strategies are superimposed on the results from the literature. In the legend, "Coast-Down," "Spin-Up," "Quasi-Steady Adiabatic," and "Steady Isothermal" refer to simulation type. The unsteady simulations included here employ the exponential fitting technique. Good agreement is demonstrated between the different simulation types.

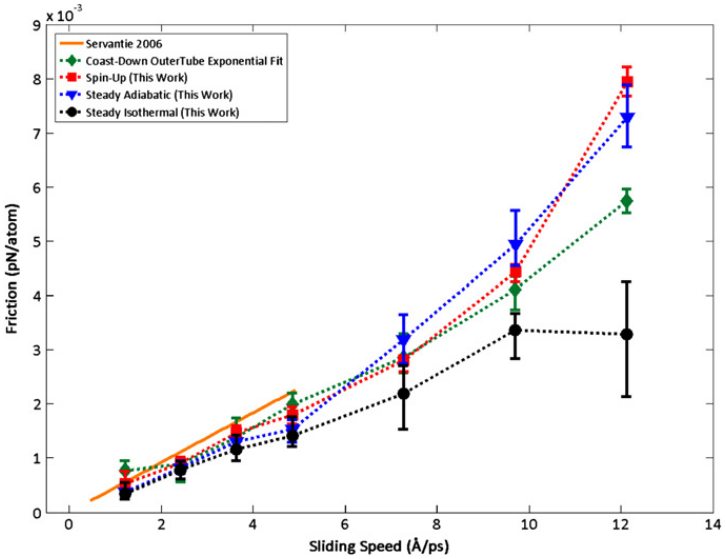

Fig. 8. The same results are shown as Fig. 7, with a linear scale, and with some literature results removed, to better show the level of agreement between simulation types. Note that while the spin-up and quasi-steady adiabatic results appear higher at higher speeds, this can be explained by the temperature accumulation inherent in these simulations, as explained in the text. The coast-down simulation experiences less temperature rise (since energy is conserved), and the isothermal simulation experiences no temperature rise (since a thermostat actively regulates temperature).

the CNT system depending on the simulation mode (*e.g.* steady state vs. transient, isothermal vs. adiabatic) but instead are artifacts introduced by inconsistencies in the implementations. If consistency of implementation is emphasized, even independent and complementary simulation methods yield the same quantitative results.

The results of each simulation are in reasonable agreement with the results of Servantie and Gaspard (2006), which is the lowest of the selected literature, and which also employs ensemble averaging. The baseline simulation also captures the same trend of the friction, namely a linear dependence on speed. This is remarkable, in particular because the baseline simulation is a steady state simulation, whereas the work by Servantie and Gaspard employs unsteady methods.

The other three studies show greater deviations from our results, and from the results of Servantie and Gaspard. Omata et al. (2005) mentioned several possibilities that could contribute to increased friction in their adiabatic coast-down simulation. The first is related to their initial condition. They observed large oscillations in the rotational speed of the coasting CNT, which they attribute to kinetic energy being converted into potential energy and back. Such potential energy could be stored in torsion or other deformations of the CNT. In this work, similar transient oscillations were sometimes seen when the end of a CNT was suddenly rotated, and the rest of the tube had to "catch up." This effect could therefore be reduced or eliminated by waiting for such transients to damp out. Omata et al. also suggest that a non-adiabatic boundary condition could reduce the effect, since energy could leave the system rather than being stored in potential form. The second potential cause that Omata et al. give for their high friction result is the small size of their tube, which is a (4,4) CNT inside a (9,9) CNT, with an inner diameter of 0.542 nm. Such tight curvature may also increase the interaction between CNTs.

Zhu and et al. (2008) also reported higher friction values for their suite of simulations on a number of geometric configurations, including (9,9)/(14,14) and (15,0)/(23,0) systems. They emphasized the buildup of thermal energy during the adiabatic simulations, using the energy accumulation rate as a measure of the rate of frictional work; this is equivalent to the adiabatic quasi-steady simulations performed for this work. We have noted that the temperature rise due to this extra accumulated energy can cause an increase in friction, since the increased motion of the atoms enables them to interact more strongly. However, since Zhu et al. reported only slight temperature rises (less than 10% of the original temperature) this effect is likely not strong enough to explain the full amount of the difference. Another potential cause for the higher values is the method whereby the energy accumulation was tallied. Zhu et al. considered changes in the relative kinetic energy, which is defined as the total kinetic energy minus the kinetic energies due to orderly rotation and translation, whereas in this work the total kinetic energy was tallied directly. For a steady state simulation, the kinetic energy in orderly rotation and translation should not change throughout the simulation (since rotation is at a constant rate and translation is prevented) and these definitions should be equivalent; however, if there were changes in these orderly kinetic energy components (for example due to transients related to starting the rotation), those changes would affect the friction calculation in the method used by Zhu et al.

Zhang et al. (2004) gave the highest estimates for friction out of the dynamic studies from the literature, for (9,9)/(14,14) and (9,9)/(22,4) CNT systems of 6 nm length. Two implementation differences are likely responsible for the differences of this estimate. First, Zhang et al. use a potential developed for graphite by Kolmogorov and Crespi (2000) to describe the inter-tube interactions, rather than the Lennard-Jones potential. As pointed out by Zhang et al., this potential may over-estimate the friction, because it is strictly applicable only to the flat planes of graphite. An effort was made to mitigate this effect by choosing a large CNT, but the effect may still contribute to the difference in result when compared to the other literature. Additionally, Zhang et al. used a Langevin-style thermostat (Langevin, 1908) to regulate the temperature of the CNT during their simulations. As we will show later in a comparison of different thermostat types, this thermostat tends to artificially inflate the friction by including a fictitious damping term to help regulate the thermal energies of the atoms.

While the results of the four simulation types performed for this work agree well with each other, in comparison to the results from the literature, the agreement is not perfect. The spin-up and steady adiabatic simulations result in distinctly higher friction estimates, particularly at higher speeds. This effect is caused by the temperature increase which takes place during these simulations. As discussed when describing the adiabatic simulations, the adiabatic boundary conditions coupled with the enforced velocity constraint on some atoms results in kinetic energy accumulating in the system, and manifesting as increased temperature. As will be shown in this section, increased temperature increases the friction. Therefore, since these simulations are measuring friction at a higher average temperature than the nominal starting temperature, the friction reported is higher. The same effect applies to the coast-down simulations, but to a lesser extent; in the coast down simulation there is no velocity constraint, so kinetic energy is not being introduced to the system, and the only temperature rise is due to the existing kinetic energy due to the initial rotation being dissipated into disorderly thermal kinetic energy.

The agreement between different simulation types can be improved by taking these temperature effects into account. One straightforward method of correcting for these effects is to non-dimensionalize the friction in such a way that it scales with the temperature. This can be done on an energy basis. Begin with the rate $\dot{E}_T$ at which energy is converted from orderly kinetic energy to disorderly thermal kinetic energy. The energy so converted during a single revolution of the CNT is

$$\Delta E_{rot} = \frac{\dot{E}_T}{\Omega/2\pi} \tag{20}$$

Since the energy rate is equal to the friction power this can be written as

$$\Delta E_{rot} = 2\pi \frac{\dot{E}_T}{\Omega} = 2\pi \frac{F_f r_I \Omega}{\Omega} = 2\pi F_f r_I \tag{21}$$

This energy can then be normalized by the thermal kinetic energy in the system:

$$E_T = N k_B T \tag{22}$$

yielding

$$F^* \triangleq \frac{\Delta E_{rot}}{E_T} = F_f \frac{2\pi r_I}{N k_B T} \tag{23}$$

This non-dimensional force describes how strong the friction is relative to the thermal energy present in the system; in other words, it is the fraction of the existing thermal energy that is produced by the work done by the friction force during each cycle. For the adiabatic simulations, the temperature increases during the simulation. As a rough approximation, the average temperature for the simulation has been used in the force non-dimensionalization.

The sliding speed can also be reported in non-dimensional terms. It is common in MD to use the Lennard-Jones unit system, which is based on the Lennard-Jones (1931) potential force field. Using parameters for carbon (Girifalco et al., 2000) of $\varepsilon = 2.39\ meV$, $\sigma = 3.41$ Å, and $m = 2 \times 10^{-23}$ g, the Lennard-Jones velocity is

$$v_{LJ} = \sqrt{\frac{\varepsilon}{m_C}} = 139\ m/s = 1.39\ \text{Å/ps} \tag{24}$$

which is comparable in magnitude to sliding motion in the CNT. We therefore define the non-dimensional velocity

$$v^* \triangleq \frac{v}{v_{LJ}} \tag{25}$$

For reference, one could also calculate the Lennard-Jones force of

$$F_{LJ} = \frac{\varepsilon}{\sigma} \tag{26}$$

which is 1.12 pN for carbon. Note that the friction forces are several orders lower than this force, which is a characteristic strength of non-bonded van der Waals interactions, and is itself much weaker than bonding forces. The friction is therefore very low compared to all other interactions in the system; this has been one of the main reasons that its measurement has been so difficult.

When applying the non-dimensionalization factors to the friction results, even better agreement is obtained, as shown in Fig. 9, since the average temperature used to non-dimensionalize the adiabatic simulation results is the measured average temperature, which is higher than the nominal or initial temperature. In this way, the non-dimensionalization corrects for the temperature effects inherent in these simulations; this is particularly evident when comparing the two (isothermal and adiabatic) steady simulations.

One of the primary goals of this paper is to establish the governing principles for friction in the CNT system. Part of that is the ability to express analytical relationships between friction and the various parameters on which it depends. So far, friction has been plotted as a function of speed; we begin therefore with the dependence of friction on the speed of the

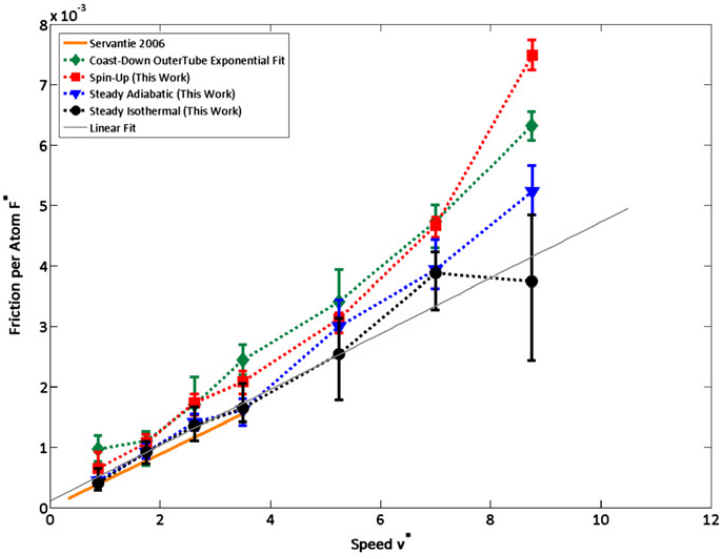

Fig. 9. When non-dimensionalized by the thermal kinetic energy the dependence of friction on sliding speed is in excellent agreement across a range of simulation styles, particularly for low speeds. The gray line is a least squares linear fit of the isothermal steady simulations.

contact. For the unsteady simulations, the dependence of friction on velocity needed to be implicitly specified *a priori* in order to fit the angular momentum evolution; friction independent of speed was assumed for a linear fit, and friction directly proportional to speed was assumed for the exponential fit. However, we would like to determine the relationship without making these assumptions *a priori*. To that end, we must use the steady-state simulations. These are the only simulations in which the speed is held constant for the entire simulation, and hence for which the friction is truly measured at a particular speed. Furthermore, we expect that friction will depend on temperature; since the steady state isothermal simulations are the only ones that control temperature for the simulation duration, the fit will be based on these results.

Examination of the steady isothermal simulation curve in Fig. 7 suggests a linear dependence, consistent with the assumptions made in the unsteady simulations reported here, as well as by Servantie and Gaspard (2006). A fit of the baseline simulations yields the relation.

$$F^* = A\nu^* + B \tag{27}$$

with the dimensionless coefficients being:

$$A = 4.62 \times 10^{-2}, \quad B = 1.08 \times 10^{-2} \tag{28}$$

3.2. Parametric studies

The significant differences in estimated friction values among the literature reports is partially due to differences in the underlying parameters of the simulations, and in some cases a lack of control over or measurement of these parameters. In order to be able to accurately predict the friction in the CNT bearing, it is necessary to control all the parameters that influence that friction. To that end, the simulations reported here employ techniques to ensure that each parameter is controlled as well as measured, so that the results are consistent and comparable.

It is important also to go further, to identify the dependency of the resulting friction measurement on the parameters of interest. Some parameters may not have a strong influence, implying that tight control over them is not as critical; others may be more important. Identifying the functional dependence is also useful where possible, in order to allow corrections to be made, or for eventual applications, to tailor the properties of the CNT bearing to optimize the performance. Therefore, a series of simulations (listed in Table 2) have been performed, testing the dependence of the friction on the parameters that are expected to have an influence.

3.3. Thermostat effects

One possible mechanism whereby the results could be modified in a non-physical way is in the thermostating. While the adiabatic simulations do not employ a thermostat, the other steady state simulations do, in order to maintain a constant temperature and to allow energy to pass out of the system as heat. These thermostats achieve the required temperature changes by directly altering the velocities of atoms within the simulation. This is not something that actually happens in nature, but rather an artificial way if imposing a constant temperature boundary condition. Thermostats can therefore introduce unwanted effects if not used properly. Three thermostating methods were evaluated:(Langevin (1908); Schneider and Stoll, 1978), Berendsen et al. (1984), and Nosé–Hoover (Hoover, 1985; Nosé, 1984; Shinoda et al., 2004) thermostats.

Fig. 10 gives a comparison of the three different thermostat styles with the adiabatic simulations. Recall that the adiabatic simulations do not employ a thermostat. The data show that the Berendsen and Nosé–Hoover thermostats agree to within the error bars over the entire range, and further agree within the error bars with the adiabatic simulations for the

Table 2
Parameters investigated for their effects on CNT friction.

Parameter	Range investigated	Effect on friction
Speed	25–250 GHz (ν^* between 1 and 9)	Friction varies proportionally with speed
Temperature	150–450 K	Friction varies proportionally with temperature
Tube interface radius	0.439–0.772 nm	None in that range
Inter-tube spacing	0.319–0.337	Friction increases with decreased spacing
Chirality	(4,4)/(9,9), (15,0)/(23,0) (9,9)/(14,14), (9,9)/(22,4)	None observed
Simulation technique (boundary/initial conditions)	Steady isothermal Quasi-steady adiabatic Coast-down (adiabatic) Spin-up (adiabatic)	None at speeds below 100 GHz; above 100 GHz friction increased for adiabatic simulations due to temperature increase
Thermostating implementation	None (adiabatic) Nosé–Hoover (Hoover, 1985; Nosé, 1984); Berendsen et al. (1984); Langevin (1908)	None for Nosé–Hoover or Berendsen, artificially inflated friction for Langevin, temperature effects increase friction for adiabatic case above 100 GHz

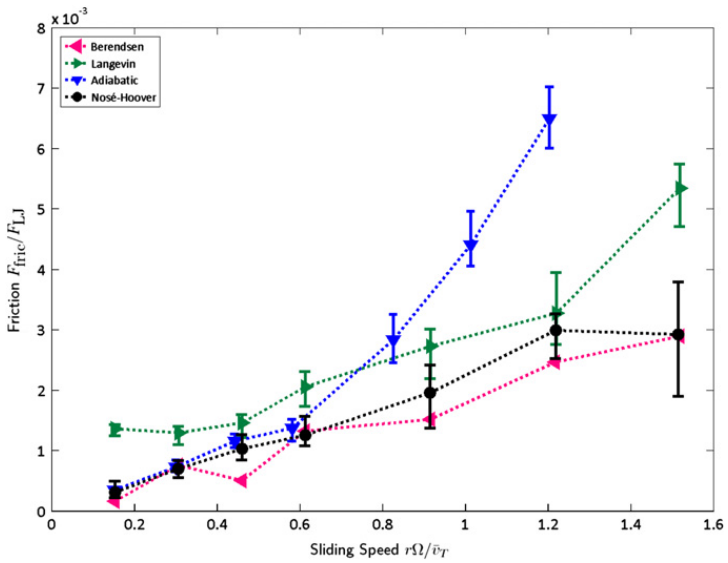

Fig. 10. Comparison of various thermostating techniques with the baseline (unthermostated, adiabatic) simulations. The adiabatic simulation appears to have higher friction at higher speeds, but this is explained by the accumulation of energy in that simulation type, as described in the text. Good agreement is demonstrated between the Berendsen and Nosé–Hoover thermostats, while the Langevin thermostat overestimates friction due to the fictitious damping term.

lower speed range. This indicates that these two thermostats have a negligible influence on the dynamics of the system (at least compared to the measurement precision), and the measured friction can be independently confirmed. The deviation between the adiabatic simulations and the thermostated simulations at high speeds can be attributed to temperature effects. At higher speeds, the amount of thermal energy that builds up during the simulation is substantial due to the high friction, and the temperature actually increases significantly during the simulation, causing the friction to increase. In these cases, the thermostated simulations should be considered more accurate, as they control the temperature at a constant value.

It is however troubling that the Langevin thermostat does not give similar results to the other two thermostats. When used, the Langevin thermostat causes the friction to be consistently high by an order of magnitude. The apparent increase in friction is likely a result of the fictitious damping term introduced by the Langevin thermostat; this term causes additional energy to be removed from the simulation at each time step, beyond that dissipated by the friction. The other thermostat results should therefore be considered more accurate; that is the reason the Nosé–Hoover thermostat was used for the baseline and all other simulations.

3.4. Temperature effects

Fig. 11 illustrates the effect of temperature on the friction. Three cases, thermostated at 150 K, 300 K, and 450 K are shown; these use the Nosé–Hoover thermostat to regulate the temperature. Temperature does significantly influence the magnitude of the friction. The effect is intuitive; for higher temperatures, the atoms are vibrating randomly with higher amplitudes, making it easier for atoms to collide during rotation, transferring their orderly kinetic energy into increased temperature. Based on the plot, the dependence of friction on temperature appears approximately linear. This linear dependence of friction on the temperature is the reason that friction has been non-dimensionalized by a factor that varies linearly with temperature (specifically the thermal energy); doing so allows results from different temperatures to collapse onto a single trend.

3.5. Chirality effects

Chirality is a unique property of CNTs, which describes the helical angle at which a graphene sheet must be rolled in order to produce a given CNT. The chirality can be completely described by two numbers, called the chiral indices, denoted by (m,n). Detailed descriptions of how the chiral indices determine the CNT geometry are readily available (Dresselhaus and Avouris, 2001). It has been hypothesized that the chirality may affect CNT friction (Guo and Gao, 2005; Servantie and Gaspard, 2006; Zhang et al., 2004), because the ridges in the energy landscape may interlock more easily when the threads of the two tubes align. Additionally, the chirality of tubes tested has varied amongst the friction reports in the literature, and may contribute to the variation in reported friction values. For that reason, the friction in CNT systems of different chiralities was simulated. Four different chiralities were chosen, based on the four chiralities used in the literature studies (Omata et al., 2005; Servantie and Gaspard, 2006; Zhang et al., 2004; Zhu and et al., 2008) selected as most relevant (as

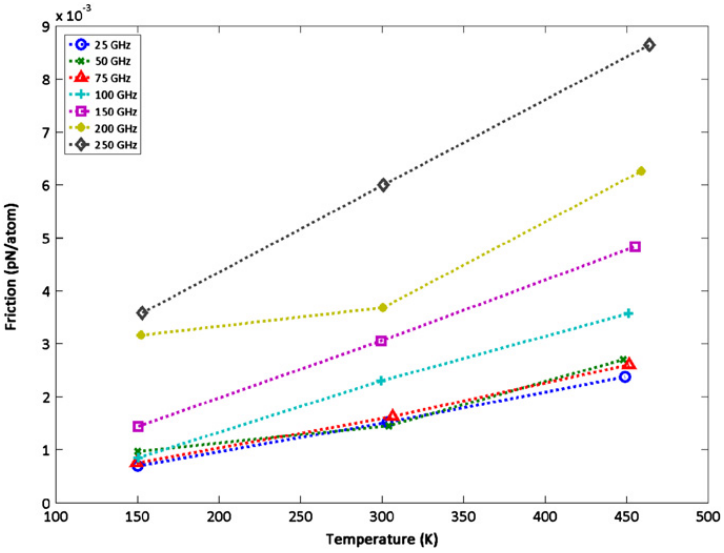

Fig. 11. Dependence of friction on simulation temperature. These steady isothermal simulations use a Nosé–Hoover thermostat to regulate the temperature. Friction varies linearly with temperature.

Table 3
Comparison of CNT geometries used in the literature*.

Inner tube	Outer tube	Inner tube radius (nm)	Outer tube radius (nm)	Interface radius (nm)	Spacing (nm)	Investigated by
(4,4)	(9,9)	0.2733	0.6055	0.4394	0.3322	(Omata et al., 2005; Servantie and Gaspard, 2006)
(15,0)	(23,0)	0.5795	0.8984	0.7390	0.3189	(Zhu and et al., 2008)
(9,9)	(14,14)	0.6034	0.9398	0.7716	0.3363	(Zhang et al., 2004)
(9,9)	(22,4)	0.6035	0.9404	0.7719	0.3370	(Zhang et al., 2004)

* Radii were measured from the simulations, not estimated from chiral indices, or taken from literature.

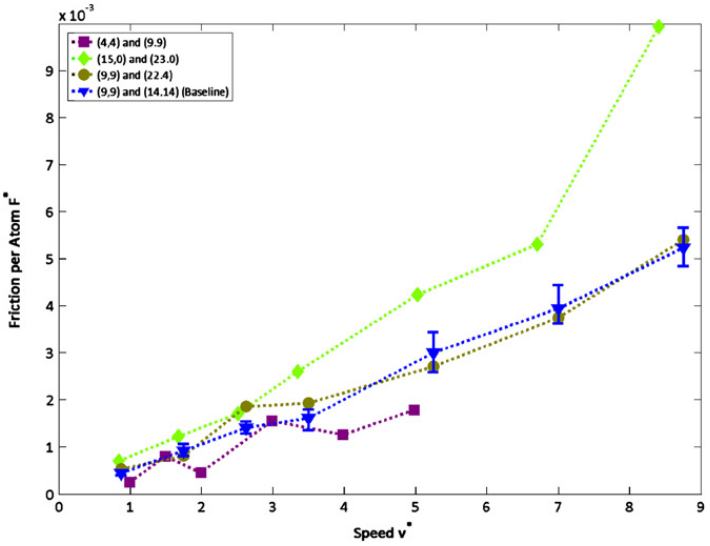

Fig. 12. Effect of different CNT chiralities is investigated, using quasi-steady adiabatic simulations. Each chirality has an associated interface radius (characteristic of the overall tube size) and spacing (between the two tubes) which are listed in Table 3. Chirality does not have a strong effect at lower speeds, and the data agree well for different CNTs. However, at higher speeds, the tube with tighter spacing ((15,0) and (23,0)) tends to experience increased friction, likely due to the increased strength of the interaction between tubes when the spacing is reduced.

explained in the Introduction.) These four chiralities are listed in Table 3, and the results of the corresponding friction simulations are illustrated in Fig. 12.

When considering chirality, however, there are two complicating factors that must be considered. Because the chirality completely specifies the CNT geometry, the radius of a given CNT is also known based on the chirality, and can be

estimated directly from the chiral indices. For a DWNT, that means that both the interface radius r_I and the inter-tube spacing are determined by the chirality. Care must therefore be taken to isolate the effect of chirality alone from the effects of CNT interface radius and spacing. The interface radius and spacing for the chiralities used are recorded in Table 3, based on measurements from the simulations.

The interface radius, which is half of the average diameter between the two CNTs, might be expected to have an effect on the friction in the CNT system. Large diameter CNTs have a lower curvature than smaller diameter, which means that less bending energy is required per atom in the tube to maintain that curve. Additionally, the greater number of atoms around the circumference means that larger deflections are possible. These two factors contribute to a softer CNT, and it might be expected that this reduced stiffness could cause an increase in friction, by encouraging the transfer of kinetic energy into thermal vibrations of the atoms.

The spacing also might be expected to influence the friction; for tighter spacings, the energy minimum at the equilibrium spacing is shallower, and the energy gradient is steeper (and hence the forces are stronger.) This stronger interaction would be expected to increase friction for tighter spacings.

In fact, however, the data (Fig. 12) show that these two effects, along with any effect that might be present due to chirality alone, are only present at higher rotational speeds. For sliding speeds lower than $v^*=3$ (about 5 Å/ps), the friction for CNTs of all four chiralities agree quite well, whereas the friction diverges for higher speeds. The deviations at higher speeds are might be explained by the spacing variations; the configuration showing the highest friction (the (15,0)/(23,0) system), has 4% less spacing than the next tightest system, and likewise the other three tubes (with very similar spacings, within 1%) do not show as much variation. The interface radius, on the other hand, does not appear to correlate with the friction results. It is also interesting to note that the interface radius dependence is consistent with simulations of friction in graphene (which is the equivalent of an infinite interface radius), as discussed in the next section. Furthermore, there is strong evidence that the chirality may not be important to the friction: for the (9,9)/(14,14) and (9,9)/(22,4) geometries, which are nearly identical in interface radius and spacing (less than 0.2% difference), there is no marked difference outside of the error bars for the entire speed range.

These results are important in establishing the basic relationships between the geometry (as described by the chiral indices) and the friction. Still, as mentioned previously, the interactions between chirality, interface radius, and spacing effects are complex, and an exhaustive probing of this parameter space was outside the scope of the paper. Further work is necessary to fully characterize the individual influences of each of these effects, as well as how they interact with each other.

3.6. Phonon computations

In addition to simulating the motion of CNTs, with the intent of measuring the friction and its dependence on various simulation parameters, it is desirable to gain some deeper understanding of the mechanism whereby friction occurs in these systems. One way to better understand the underlying phenomena is to compute and observe the phonons in the system. In particular, the power spectrum, showing to what extent phonons at each frequency contribute to the total energy in the system, can illustrate which modes contribute most strongly to the friction.

A method exists to compute the phonons, taking into account the actual motion of the system (Kong, 2011; Kong et al., 2009; FixPhonon webpage, http://code.google.com/p/fix-phonon). This code has been made available as an add-in to LAMMPS (2011). This method makes use of the equipartition theorem, which states that at equilibrium, energy is equally stored in thermal, kinetic, and potential forms. The spring constants that make up the dynamical matrix can therefore be derived by comparing the computed thermal energy with the potential energy due to displacements of the atoms from their equilibrium positions in the crystal (the spring forces of the atomic interactions). The density of states (which in fact reflects the changes in occupation of these states due to the actual motion of the tube, since the matrix was inferred from the actual moving tube) is computed by integrating the phonon dispersion relation across the wave number vectors making up the spatial decomposition. The method has also been well validated against known analytical solutions, other codes, and experimental data (Kong, 2011). Other phonon-based methods also exist for analysis of these systems (Raghunathan et al., 2011; Xu et al., 2008), and may be of interest for future work on CNT friction.

We hypothesize that the spectral density calculations will reveal which frequencies are most active in an individual tube, appearing as peaks in the power spectrum. Furthermore, we expect that these peaks might change as different effects are applied to the tube. For example, when two tubes are in contact, their interactions may damp some modes while reinforcing others. Once the tubes are rotating, the power spectrum may change again, exhibiting peak shifts due to the interactions that make up the friction between tubes. We further expect that these shifts might depend on operating conditions, such as the rotational speed or temperature, since the friction force depends on these parameters.

3.7. Phonon speed dependence

To establish an operating procedure for the phonon computation method, the power spectrum was computed for the baseline geometry, without rotation, at 300 K. The power spectrum was also computed for each tube individually, in isolation, to determine how the interaction between the two tubes affects the phonon population. These spectra are shown in Fig. 13. For reference, we have included the in-phase and out-of-phase radial breathing mode frequencies (3.7 THz and

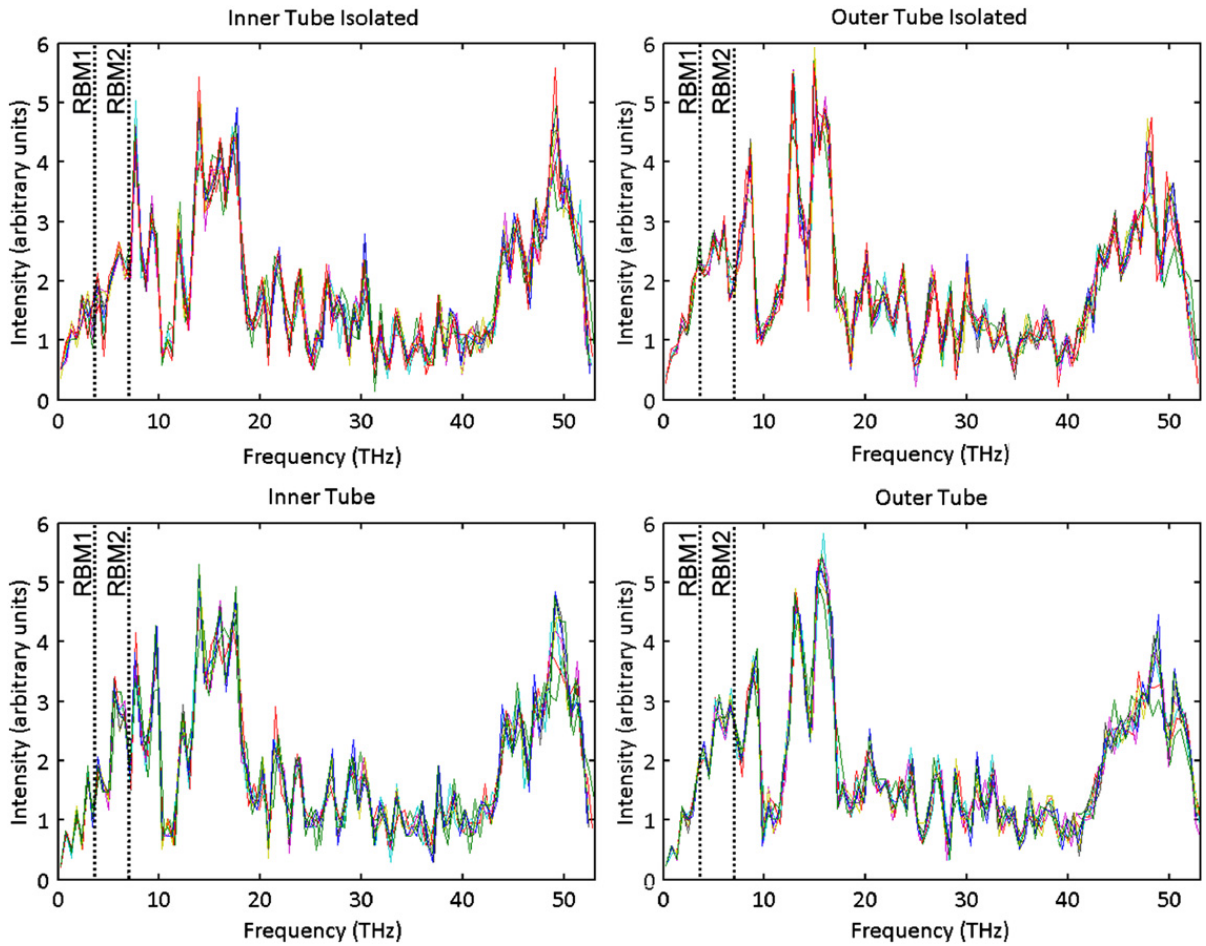

Fig. 13. Example phonon power spectra for a (9,9) CNT within a (14,14) CNT. The top row shows the power spectrum for each tube including the interactions with the other tube, while the bottom row shows the spectrum for that tube in isolation. Each spectrum was measured 6 times, and the results are overlaid in different colors. These spectra show that the distribution of energy amongst the modes is not altered by the presence of an adjacent CNT. For reference, the in-phase and out-of-phase radial breathing mode frequencies (RBM1 and RBM2, respectively) are also marked.

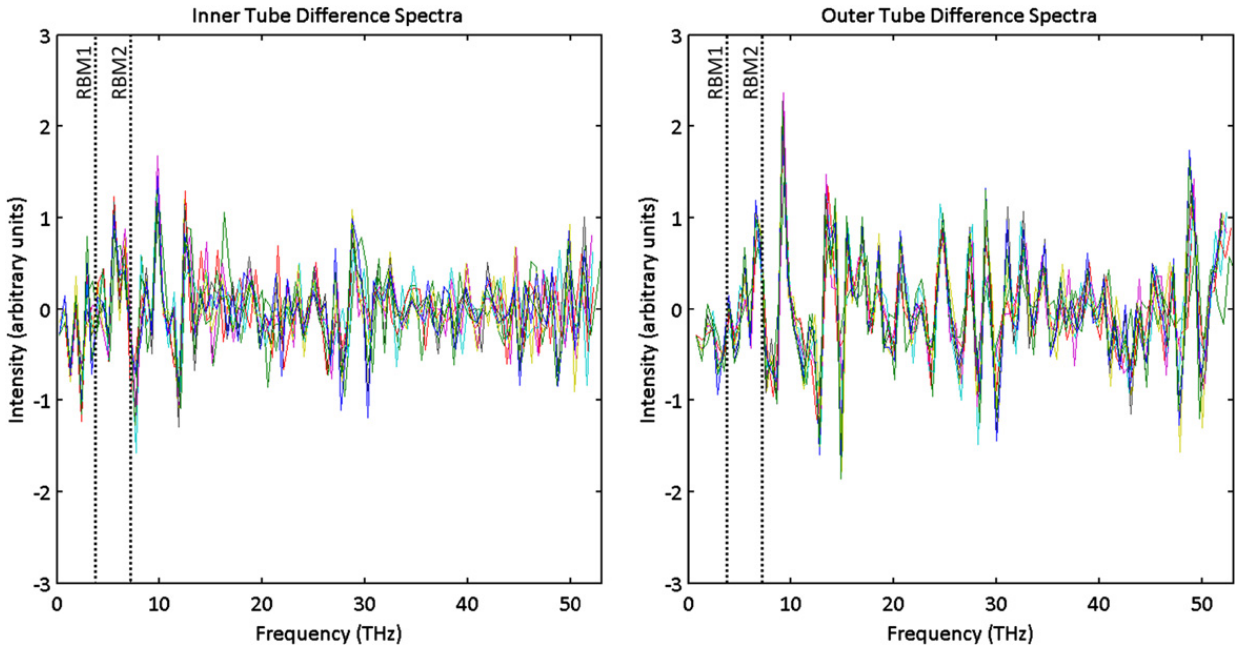

Fig. 14. Difference spectra, showing the subtraction of the isolated tube spectra from their respective interacting spectra. Each colored line corresponds to a different integration window in the simulation, all of length 1 ns. These spectra differences illustrate that adding another CNT adjacent to the original CNT does not redistribute the thermal energy across the frequency range. For refererence, the in-phase and out-of-phase radial breathing mode frequencies (RBM1 and RBM2, respectively) are also marked.

7.1 THz, respectively, for our (9,9)/(14,14) system), as calculated based on simple empirical relations from Dobardžić et al. (2003). At first glance, it appears that there is no significant difference between the tube spectra, when comparing the isolated tube to the tube with interactions. However, the changes in the spectrum might be highlighted by taking the difference of the two spectra. This difference is shown in Fig. 14. There are a few peaks that could potentially be identified, but still, in general, the differences are broadly spread across the spectrum. This would indicate that there are no particular phonon modes (at either the low-frequency end, such as the radial breathing modes, or for any particular higher order modes) that are excited or damped more than others are, due to this simple tube-tube interaction.

Phonons have also been computed for spinning tubes in the adiabatic constant velocity experiment.

Fig. 15 shows these spectra with the component from a still tube subtracted off. In order to confirm that the integration length for these spectra (chosen to be 1 ns, as is used prior literature (Thomas et al., 2010)) is sufficiently long that it captures a representative sample, two techniques were employed. First, the spectra were computed many times in a simulation, with integration windows at different points (but always of length 1 ns); after the initial transient the spectra agreed to within the level of the noise in the spectra, as can be seen in Fig. 15. Additionally, a shorter integration window (0.1 ns) was attempted; results were again identical.

The spectra differences give insight into which modes are most excited during rotation. Most of the action occurs in the neighborhood of 10–25 THz for both the inner and the outer tube, with especially strong differences between 18 and 25 THz. While these "mesas," comprising frequency ranges, do not identify individual modes, they are helpful in showing what frequency ranges are most affected by rotation. Additionally, with increasing rotation speed, some of the energy within the 17–25 THz range shifts to slightly higher frequencies, while energy in the 10–13 THz range shifts to lower frequencies. We can also detect a broadening of the distribution of affected frequencies as rotation speed increases.

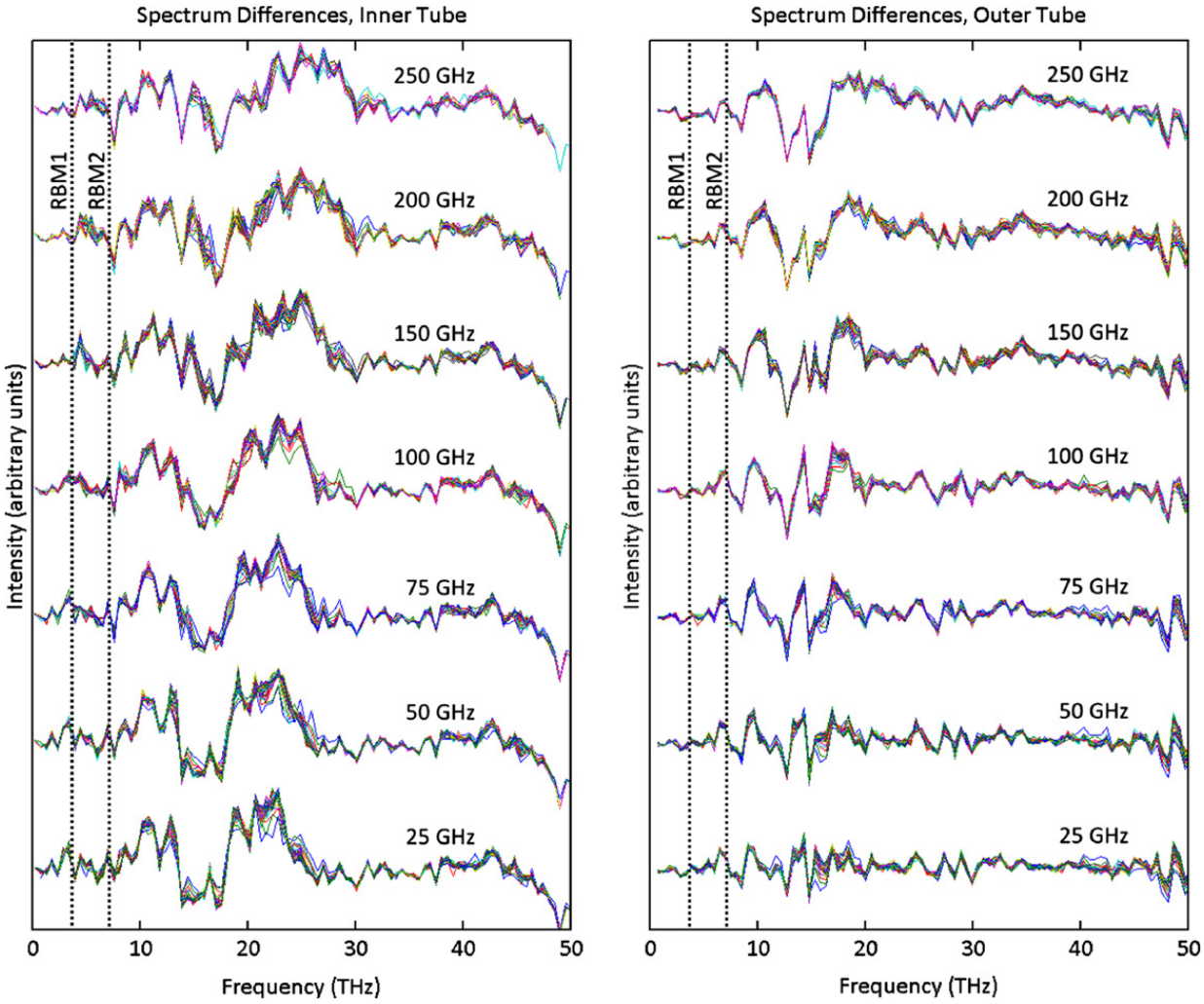

Fig. 15. The spectra of the rotating CNTs, with the spectrum of a still tube subtracted off to highlight the differences. The labels correspond to the rotational speed at which the spectra were measured, while the different colored lines each correspond to a different measurement interval, each of length 1 ns. Two regions in which there is a lot of phonon activity (9–13 THz and 17–25 THz) are visible, especially in the inner tube. These spectra show that although some frequency ranges have increased importance for the interaction between rotating tubes, the effect cannot be isolated to a particular mode or type of motion. For refererence, the in-phase and out-of-phase radial breathing mode frequencies (RBM1 and RBM2, respectively) are also marked.

At 25 GHz, the right group of frequencies is almost square (most evident in the inner tube spectra) while it becomes much smoother at higher speeds. This result would seem to indicate that the interaction between tubes is even less confined to a particular mode, and more broadly distributed for faster rotation. The change in shape of this group becomes more pronounced at about 100 GHz; this corresponds to the point where temperature increase due to energy accumulation in the adiabatic simulation becomes more apparent; the same effect is manifested as an increased slope in Fig. 7 at about 100 GHz. The inner tube also exhibits a clear decay in the upper frequency range, indicating that these high-frequency phonons are suppressed by the rotation.

In summary, the phonon analysis shows that the interactions between two tubes are not dominated by a particular mode or type of motion. Instead, the two tubes interact through a broadband mechanism, with energy being stored and transferred by phonons at a wide range of frequencies. Furthermore, rotation does not introduce a new specific type of motion that contributes strongly to the tube interactions. This indicates that the random thermal motions of the atoms are the dominant mechanism whereby the tubes interact, and thus the dominant mechanism in friction in the dynamic case.

3.8. Comparison with graphene

Another interesting question pertaining to the friction in the CNT is how that friction compares to friction in graphene, the planar analog of CNTS. Molecular dynamics simulations of friction involving graphene have been conducted (Bonelli et al., 2009; Filleter et al., 2009; Sasaki et al., 2009; Zadeh et al., 2012), but these have typically addressed friction between graphene and another object such as a C60 molecule or a nanoindenter probe tip. Here, friction between two adjacent graphene sheets is simulated. In the limit of increasing tube diameter, the CNT bearing system becomes equivalent to a graphene system, wherein two infinite sheets of graphene are translating relative to each other. This situation was also simulated, for comparison. The geometry (shown in Fig. 16) consisted of two graphene sheets, corresponding to unwrapped (5,5) CNTs with a length of 10 hexagons, or a rectangle of dimensions 21.2 Å by 24.5 Å, with periodic boundary conditions to simulate an infinite sheet. A coast-down experiment was performed, where the top sheet was given an initial translational velocity, and the bottom sheet is prevented from sliding by fixing a single corner atom to have no displacements in the plane of the graphene sheet. This boundary condition was meant to be analogous to the CNT case, where a few atoms on the CNT end are constrained Again, the time rate of change of the momentum (translational momentum, in this case) is equal to the friction force.

The resulting friction data, from the graphene simulation (shown in Fig. 17) illustrates that the friction in graphene is in quantitative agreement with that measured for CNTs; although there is a very large variability in the measurements (likely caused by the small simulation domain used to reduce computational cost), the results fall within the error bars of the CNT friction for most cases, the general trend can be inferred to be the same. This observation reinforces the findings from the simulations of CNTs of different diameters, that the friction does not depend strongly on the CNT diameter. Indeed, graphene corresponds to a CNT of infinite diameter, which is the limiting case.

While it has been expected that graphene friction should behave in the same way as CNT friction, this novel result demonstrates that it does agree quantitatively. The implications of such a finding are important for several reasons. First, the graphene simulations are much simpler to set up and implement, because they do not incorporate rotation but only translation. It is therefore unnecessary to decompose individual atom velocities based on their position in order to derive the tangential components, as is necessary in the CNT simulation to compute the temperature correctly and to measure the angular momentum and kinetic energy. The graphene simulation also runs more quickly as a result of doing away with

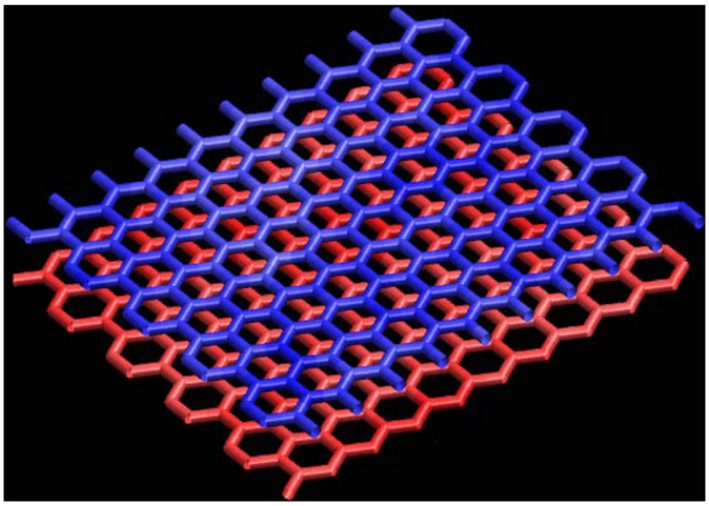

Fig. 16. Geometry for the graphene simulations consisted of two rectangular graphene sheets with a periodic boundary condition in both in-plane directions.

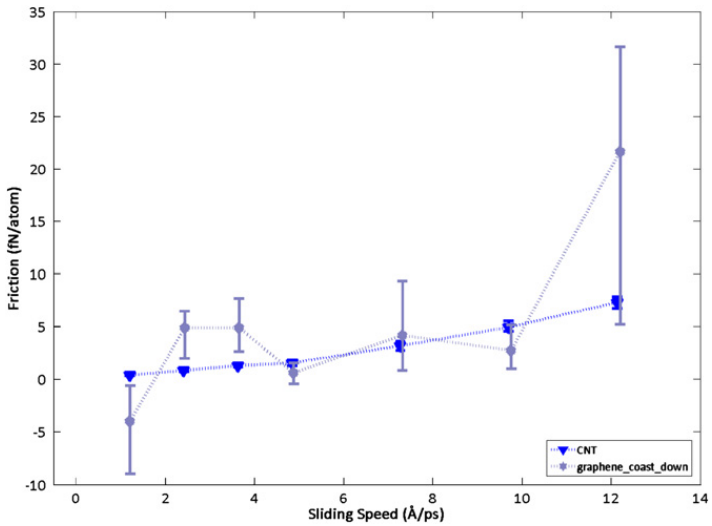

Fig. 17. Friction in the graphene system, as a function of relative sliding speed. The baseline CNT simulations are also shown for comparison. The larger error bars are likely due to the small size of the simulated graphene system, which does not provide for as many atoms across which to average the data. Graphene appears to have friction quantitatively similar to CNTs as expected.

these extra per-atom computations. It would therefore be beneficial to use graphene simulations to gather a large dataset on friction instead of CNT simulations, to save computational cost.

More importantly, use of graphene may aid in developing a better understanding of the mechanisms driving the friction. The mode shapes in graphene are simpler, corresponding to waves in two dimensions, instead of complex, fully three-dimensional shapes. If the modes contributing to friction in graphene can be established, it would be straightforward to visualize the same of these modes, which could show exactly what atomic motions cause the friction. For example, is there a stick–slip interaction in which atoms transfer their in-plane kinetic energy, or does energy transfer occur by coupling of out-of-plane vibrations? Removing the complicating factors due to the cylindrical nature of the CNT should make it easier to see the mechanisms at work. Future research on friction in carbon systems, particularly research aimed at developing a better understanding of the mechanisms, should take advantage of the simpler graphene system to gain better insight.

4. Conclusions

This work has addressed the discrepancies among CNT friction estimates reported in the literature. By conducting many different types of simulations with carefully controlled parameters, it has been shown that the independent simulations types can produce results within each other's error bars (and average values differing by a factor of two or three), and need not differ by several orders of magnitude as had previously been reported. The work focused on rotating CNT bearing systems, thereby specifically avoiding issues related to van der Waals restoring forces, edge effects, and coupling between rotation and translation that would more strongly affect behavior in telescoping or translating CNT bearing friction systems.

In addition, the effects of an array of parameters on the CNT friction have been investigated. While the friction does not depend on the simulation approach (and should not, since friction is a property of the system and not of the particular simulation designed to probe that system), friction has been found to depend on other parameters. Friction appears to vary linearly with sliding speed (as in viscous damping), for the range of speeds considered. This was consistent across all types of simulations considered, when accounting for the temperature increase inherent in adiabatic simulations. Friction also depends linearly on temperature, as seen not only in steady state simulations with controlled temperature, but also in adiabatic simulations where the temperature increases because kinetic energy is dissipated into thermal energy. Increased temperature leads to increased friction because the amplitude of the thermal vibrations is higher, leading to more collisions between atoms, and hence more transfer of energy from orderly kinetic energy into disorderly thermal motion. Geometric considerations were found to have weaker effects; the tube interface radius and chirality did not cause deviations in friction larger than the measurement error. Chirality has a strong effect in the quasi-static simulations reported by the literature, because it directly alters the potential energy landscape, but both chirality and mean radius do little to alter the interactions of thermal vibrations, which is the main friction mechanism in the dynamic case. Conversely, friction was found to increase with decreasing inter-tube spacing, since the tighter spacing increases the stiffness of the van der Waals interaction between the atoms of adjacent tubes. Because of the complex inter-relationship between chirality, interface radius, and spacing, the exact nature of these dependencies could not be determined from the limited data acquired here; further study on this point is required. The other geometric parameter, tube length, which is independent of the other three, also did not appear to influence the value of friction *per atom* (total friction scales with the

number of atoms), although longer tubes experienced higher variability from run to run (a tube four times longer shows error bars two to three times larger), because of the increased tube softness, which makes excitation of bending modes easier.

Graphene was also shown to exhibit qualitatively similar friction behavior to CNTs, as is expected, since graphene is a planar analog of the CNT. Because of this similarity, graphene might prove to be a useful test system for further CNT friction study, especially since the computational cost is reduced and geometry and simulation implementation are simplified compared with the CNT. This could motivate future experimental and computational studies.

Finally, the mechanisms behind the friction have been investigated by studying the phonons that make up the motion in the CNT bearing system. It has been found that stationary CNTs display little difference in phonon spectra (the difference between spectra is everywhere less than half of the amplitude of the original spectra, and does not exhibit any clear peaks, valleys, or plateaus) depending on whether an inner or outer tube is present and exerting van der Waals interactions on it. When comparing the spectrum of a rotating tube to the still tube, the difference of the spectra exhibit some plateaus of activity in the range of 10–14 THz and 20–25 THz, but no specific frequency peaks, indicating that the mechanisms for dissipating orderly kinetic energy into disorderly thermal energy are broadband, and not linked to any one particular mode strongly. It may therefore difficult to "engineer" the friction by controlling the CNT geometry in order to modify certain phonons. A new and important result is that friction in CNTs is dominated by the broadband interactions of thermal vibrations, and not by a specific type of atomic motion.

Acknowledgments

This work was supported in part by NSF.

Appendix A. Supporting information

Supplementary data associated with this article can be found in the online version at http://dx.doi.org/10.1016/j.jmps.2012.08.004.

References

Akita, S., Nakayama, Y., 2003. Interlayer sliding force of individual multiwall carbon nanotubes. Jpn. J. Appl. Phys. 42, 4830–4833.
Akita, S., Nakayama, Y., 2005. Mechanical and electrical properties of multiwall nanotube under interlayer sliding. e-J. Surf. Sci. Nanotechnol. 3, 86–93.
Berendsen, H.J.C., Postma, J.P.M., Gunsteren, W.F.v., DiNola, A., Haak, J.R., 1984. Molecular dynamics with coupling to an external bath. J. Chem. Phys. 81 (8), 3684–3690.
Bonelli, F., Manini, N., Cadelano, E., Colombo, L., 2009. Atomistic simulations of the sliding friction of graphene flakes. Eur. Phys. J. B—Condens. Matter Complex Syst. 70 (4), 449–459.
Bourlon, B., Glattli, D.C., Miko, C., Forro, L., Bachtold, A., 2004. Carbon nanotube based bearing for rotational motions. Nano Lett. 4 (4), 709–712.
Brenner, D.W., 1990. Empirical potential for hydrocarbons for use in simulating the chemical vapor deposition of diamond films. Phys. Rev. B 42 (15), 9458–9471.
Charlier, J.C., Michenaud, J.P., 1993. Energetics of multilayered carbon tubules. Phys. Rev. Lett. 70 (12), 1858–1861.
Cumings, J., Zettl, A., 2000. Low-friction nanoscale linear bearing realized from multiwall carbon nanotubes. Science 289 (5479), 602–604.
Dobardžić, E., Maultzsch, J., Milošević, I., Thomsen, C., Damnjanović, M., 2003. The radial breathing mode frequency in double-walled carbon nanotubes: an analytical approximation. Phys. Status Solidi (b) 237 (2), R7–R10.
Dresselhaus, M., Avouris, P., 2001. Introduction to carbon materials research. In: Dresselhaus, M.S., Dresselhaus, G., Avouris, P. (Eds.), Carbon Nanotubes: Synthesis, Structure, Properties, and Applications. Springer-Verlag, New York, pp. 1–9.
Fennimore, A.M., Yuzvinsky, T.D., Han, W.Q., Fuhrer, M.S., Cumings, J., Zettl, A., 2003. Rotational actuators based on carbon nanotubes. Nature 424 (6947), 408–410.
Filleter, T., McChesney, J.L., Bostwick, A., Rotenberg, E., Emtsev, K.V., Seyller, T., Horn, K., Bennewitz, R., 2009. Friction and dissipation in epitaxial graphene films. Phys. Rev. Lett. 102 (8), 086102-1–086102-4.
FixPhonon webpage, http://code.google.com/p/fix-phonon/.
Girifalco, L.A., Hodak, M., Lee, R.S., 2000. Carbon nanotubes, buckyballs, ropes, and a universal graphitic potential. Phys. Rev. B 62 (19), 13104–13110.
Guo, W., Gao, H., 2005. Optimized bearing and interlayer friction in multiwalled carbon nanotubes. Comput. Modeling Eng. Sci. 7 (1), 19–34.
Guo, W., Guo, Y., Gao, H., Zheng, Q., Zhong, W., 2003. Energy dissipation in gigahertz oscillators from multiwalled carbon nanotubes. Phys. Rev. Lett. 91 (12), 125501-1–125501-4.
Guo, W., Zhong, W., Dai, Y., Li, S., 2005. Coupled defect-size effects on interlayer friction in multiwalled carbon nanotubes. Phys. Rev. B (Conden. Matter Mater. Phys.) 72 (7), 075409–075410.
Guo, Z., Chang, T., Guo, X., Gao, H., 2011. Thermal-induced edge barriers and forces in interlayer interaction of concentric carbon nanotubes. Phys. Rev. Lett. 107 (10), 105502.
Hoover, W.G., 1985. Canonical dynamics: equilibrium phase-space distributions. Phys. Rev. A 31 (3), 1695–1697.
Kis, A., Jensen, K., Aloni, S., Mickelson, W., Zettl, A., 2006. Interlayer forces and ultralow sliding friction in multiwalled carbon nanotubes. Phys. Rev. Lett. 97 (2), 025501–025504.
Kolmogorov, A.N., Crespi, V.H., 2000. Smoothest bearings: interlayer sliding in multiwalled carbon nanotubes. Phys. Rev. Lett. 85 (22), 4727–4730.
Kong, L.T., 2011. Phonon dispersion measured directly from molecular dynamics simulations. Comput. Phys. Commun. 182 (10), 2201–2207.
Kong, L.T., Bartels, G., Campañá, C., Denniston, C., Müser, M.H., 2009. Implementation of Green's function molecular dynamics: an extension to LAMMPS. Comput. Phys. Commun. 180 (6), 1004–1010.
LAMMPS, 2011. WWW Site, http://lammps.sandia.gov/.
Langevin, P., 1908. On the theory of Brownian motion. Comptes rendus de l'Acad. des Sci. 146, 530–533.
Lennard-Jones, J.E., 1931. Cohesion. Proc. Phys. Soc. 43, 461–482.

Liu, P., Zhang, Y.W., 2011. A theoretical analysis of frictional and defect characteristics of graphene probed by a capped single-walled carbon nanotube. Carbon 49 (11), 3687–3697.
Nosé, S., 1984. A unified formulation of the constant temperature molecular dynamics methods. J. Chem. Phys. 81 (1), 511–519.
Omata, Y., Yamagami, Y., Tadano, K., Miyake, T., Saito, S., 2005. Nanotube nanoscience: a molecular-dynamics study. Phys. E: Low-dimensional Syst. Nanostruct. 29 (3-4), 454–468.
Plimpton, S., 1995. Fast parallel algorithms for short range molecular dynamics. J. Comput. Phys. 117, 1–19.
Raghunathan, R., Greaney, P.A., Grossman, J.C., 2011. Phonostat: thermostatting phonons in molecular dynamics simulations. J. Chem. Phys. 134 (21), 214117-1–214117-9.
Rivera, J.L., McCabe, C., Cummings, P.T., 2003. Oscillatory behavior of double nanotubes under extension: a simple nanoscale damped spring. Nano Lett. 3 (8), 1001–1005.
Rivera, J.L., McCabe, C., Cummings, P.T., 2005. The oscillatory damped behaviour of incommensurate double-walled carbon nanotubes. Nanotechnology 16 (2), 186–198.
Salehinia, I., Medyanik, S.N., 2011. Transmission between translational and rotational motions in double-walled carbon nanotubes. J. Comput. Theor. Nanos. 8 (2), 179–188.
Sasaki, N., Saitoh, H., Terada, K., Itamura, N., Miura, K., 2009. Simulation of atomic-scale wear of graphite—nanotip induced graphene formation. e-J. Surf. Sci. Nanotechnol. 7, 173–180.
Schneider, T., Stoll, E., 1978. Molecular-dynamics study of a three-dimensional one component model for distortive phase transitions. Phys. Rev. B 17 (3), 1302–1322.
Servantie, J., Gaspard, P., 2006. Rotational dynamics and friction in double-walled carbon nanotubes. Phys. Rev. Lett. 97 (18), 186106-1–186106-4.
Shinoda, W., Shiga, M., Mikami, M., 2004. Rapid estimation of elastic constants by molecular dynamics simulation under constant stress. Phys. Rev. B 69 (13), 134103–134110.
Stuart, S.J., Tutein, A.B., Harrison, J.A., 2000. A reactive potential for hydrocarbons with intermolecular interactions. J. Chem. Phys. 112, 6472–6486.
Tersoff, J., 1988. New empirical approach for the structure and energy of covalent systems. Phys. Rev. B 37 (12), 6991–7000.
Thomas, J.A., Turney, J.E., Iutzi, R.M., Amon, C.H., McGaughey, A.J.H., 2010. Predicting phonon dispersion relations and lifetimes from the spectral energy density. Phys. Rev. B 81 (8), 081411-1–081411-4.
Xu, Z.P., Zheng, Q.S., Jiang, Q., Ma, C.C., Zhao, Y., Chen, G.H., Gao, H., Ren, G.X., 2008. Trans-phonon effects in ultra-fast nanodevices. Nanotechnology 19 (25), 255705-1–255705-5.
Yu, M.F., Yakobson, B.I., Ruoff, R.S., 2000. Controlled sliding and pullout of nested shells in individual multiwalled carbon nanotubes. J. Phys. Chem. B 104, 8764–8767.
Zadeh, M.J., Reddy, C.D., Sorkin, V., Zhang, Y.W., 2012. Kinetic nanofriction: a mechanism transition from quasi-continuous to ballistic-like Brownian regime. Nanoscale Res. Lett. 7, 148-1–148-8.
Zettl, A.K., Fennimore, A.M., Yuzvinsky, T.D., 2004. In: Rotational Actuator or Motor Based on Carbon NanotubesThe Regents of the University of California, USA.
Zhang, S., Liu, W.K., Ruoff, R.S., 2004. Atomistic simulations of double-walled carbon nanotubes (DWCNTs) as rotational bearings. Nano Lett. 4 (2), 293–297.
Zhang, X.H., Tartaglino, U., Santoro, G.E., Tosatti, E., 2007. Velocity plateaus and jumps in carbon nanotube sliding. Surf. Sci. 601 (18), 3693–3696.
Zhu, B.E., et al., 2008. Thermal effect on DWCNTs as rotational bearings. Nanotechnology 19 (49), 495708-1–495708-5.